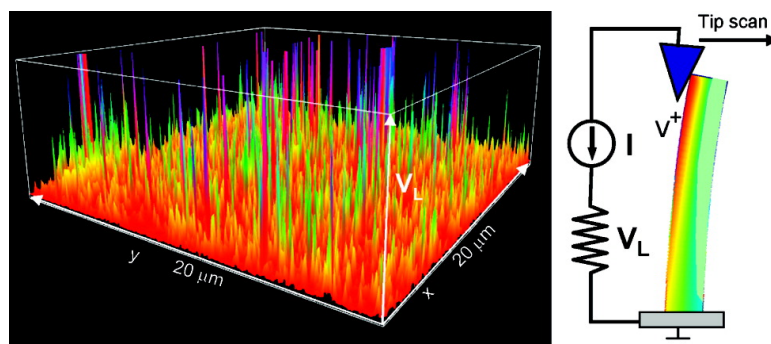


Piezoelectric Nanogenerator Using p-Type ZnO Nanowire Arrays

Ming-Pei Lu, Jinhui Song, Ming-Yen Lu, Min-Teng Chen, Yifan Gao, Lih-Juann Chen, and Zhong Lin Wang

Nano Lett., 2009, 9 (3), 1223-1227 • DOI: 10.1021/nl900115y • Publication Date (Web): 11 February 2009

Downloaded from <http://pubs.acs.org> on March 11, 2009



More About This Article

Additional resources and features associated with this article are available within the HTML version:

- Supporting Information
- Access to high resolution figures
- Links to articles and content related to this article
- Copyright permission to reproduce figures and/or text from this article

[View the Full Text HTML](#)

Piezoelectric Nanogenerator Using p-Type ZnO Nanowire Arrays

Ming-Pei Lu,^{†,||} Jinhui Song,^{‡,||} Ming-Yen Lu,^{‡,§} Min-Teng Chen,[§] Yifan Gao,[‡] Lih-Juann Chen,[§] and Zhong Lin Wang^{*,‡}

National Nano Device Laboratories, Hsinchu, Taiwan 30078, Republic of China, School of Materials Science and Engineering, Georgia Institute of Technology, Atlanta, Georgia 30332, and Department of Materials Science and Engineering, National Tsing Hua University, Hsinchu, Taiwan 30043, Republic of China

Received January 13, 2009

ABSTRACT

Using phosphorus-doped ZnO nanowire (NW) arrays grown on silicon substrate, energy conversion using the p-type ZnO NWs has been demonstrated for the first time. The p-type ZnO NWs produce positive output voltage pulses when scanned by a conductive atomic force microscope (AFM) in contact mode. The output voltage pulse is generated when the tip contacts the stretched side (positive piezoelectric potential side) of the NW. In contrast, the n-type ZnO NW produces negative output voltage when scanned by the AFM tip, and the output voltage pulse is generated when the tip contacts the compressed side (negative potential side) of the NW. In reference to theoretical simulation, these experimentally observed phenomena have been systematically explained based on the mechanism proposed for a nanogenerator.

Harvesting energy from the environment is a potential approach for building self-powered nanodevices/nanosystems.^{1–9} Piezoelectric nanogenerators using nanowires (NWs) are a method for converting mechanical energy into electricity.^{8,9} NWs made of wurtzite structured materials, such as ZnO, GaN, CdS, and ZnS, are the most important candidates for the nanogenerators, among which, ZnO is the best candidate. Utilizing the semiconductor and piezoelectric property possessed by ZnO NWs, an energy generator has been demonstrated for converting mechanical energy into electricity.^{4–7} Under the straining created by an external force, a piezoelectric potential is created in the NW as a result of elastic deformation, which drives the flow of charge carriers through an external load. A Schottky barrier formed between the electrode and the NW serves as a “gate” that controls the flowing direction of the charge carriers. This is the principle of the nanogenerator.^{4,8}

All of the existing literature on nanogenerator is established using n-type ZnO NWs, while little is known about the characteristics of p-type ZnO NWs for energy harvesting. According to the theoretical study, the synthesis of p-type ZnO NWs has been proven extremely difficult.^{10,11} Only a couple of reports exist about the successful synthesis of the p-type ZnO NW.^{12,13} In this report, we have synthesized P-doped ZnO p-type NW arrays, with which the character-

istics of the piezoelectric energy conversion process of p-type ZnO NWs have been systematically investigated. A single NW has been shown to produce a piezoelectric output as high as 50–90 mV. The distinct performance of the p-type NWs for a nanogenerator has been systematically described based on the mechanism established for the nanogenerator.

The P-doped ZnO NW arrays were grown on (001) silicon substrate using a thermal vapor deposition method.¹¹ A thin film of zinc acetate was dropped on the substrate using a solution containing 20 mM zinc acetate dihydrate ($\text{Zn}(\text{C}_2\text{H}_3\text{O}_2)_2 \cdot 2\text{H}_2\text{O}$) in ethanol. ZnO thin films of thickness 100–200 nm was formed after annealing at 300 °C in air for 30 min. A mixture of ZnO powder and graphite powder with the same molar ratio was used as precursor, and different amounts of zinc phosphate (Zn_3P_2) powder were used as the dopant source. The ZnO/C sources were placed on an alumina boat and positioned in the high temperature zone of the furnace (1050 °C). ZnO-coated Si substrate was set to a fixed distance downstream from the source boat, positioned horizontally inside the tube furnace, pumped to a pressure of 1.5×10^{-2} Torr. A mixture of 100 sccm Ar and 10 sccm O_2 was used as carrier gas. The growth temperature was controlled at 600 °C and the system was kept at 0.7–1 Torr for 60 min.

Catalyst-free P-doped ZnO NW (NW) arrays were grown vertically on a Si wafer with a continuous ZnO film as a seed layer (Figure 1a). This continuous ZnO film serves as an electrode when measuring the piezoelectric responses of the p-type NWs. Cross-section samples depicting the

* Corresponding author, zlwang@gatech.edu.

[†] National Nano Device Laboratories.

[‡] Georgia Institute of Technology.

[§] National Tsing Hua University.

^{||} Authors with equal contribution.

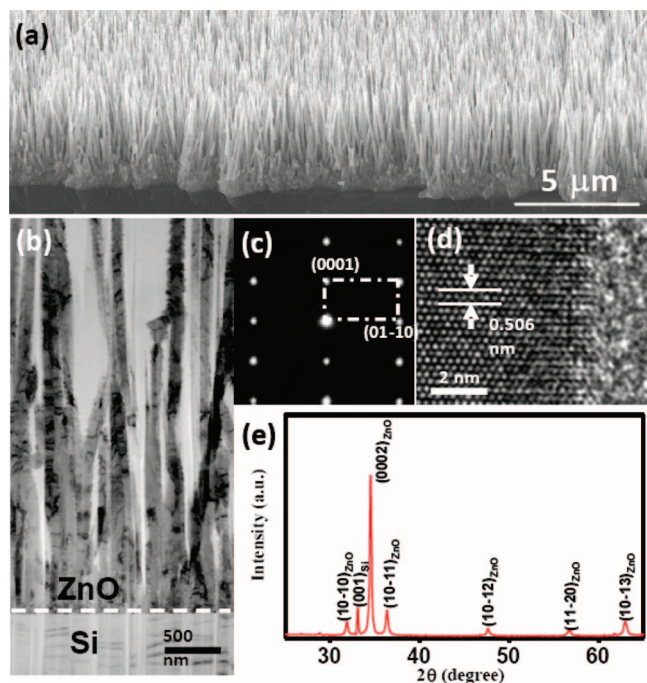


Figure 1. Morphological and structural characterization of P-doped ZnO NW arrays. (a) Low-magnification SEM image of aligned P-doped ZnO NW arrays grown on Si substrate. (b) Cross-section TEM image of P-doped NW arrays. (c) The selected area electron diffraction pattern (SAED) recorded from a single P-doped ZnO NW. (d) High-resolution TEM image recorded from the side of a P-doped NW. (e) XRD spectrum recorded from P-doped ZnO NW arrays.

NW–substrate interface were prepared using a focused ion beam (FIB) system, which sliced the sample along a direction normal to the substrate (e.g., closely parallel to the NWs); a cross-section transmission electron microscopy (TEM) image of the P-doped ZnO NW arrays grown on Si(001) substrate is presented in Figure 1b. The orientation relationships between the Si substrate and the NWs are as follows: Si(001) \parallel ZnO(0001), Si[1 $\bar{1}$ 2] \parallel ZnO[01 $\bar{1}$ 0], Si[110] \parallel ZnO[2 $\bar{1}$ 1 $\bar{0}$] (see Figure S1 in Supporting Information). The nonuniform contrast observed at the Si side in Figure 1b is due to the sample thickness variation as produced by the ion beam parallel to the NWs during sample preparation. The selected area electron diffraction (SAED) pattern (Figure 1c) from a single NW reveals its single crystal structure; the corresponding high-resolution TEM image (Figure 1d) shows clear lattice fringes of the (0001) plane of wurtzite ZnO structure. The growth direction of NWs is determined to be [0001]. Moreover, a typical X-ray diffraction (XRD) pattern of the P-doped ZnO NW arrays is shown in Figure 1e. Besides the (001) peak from the Si substrate, other peaks are all indexed to wurtzite-structured ZnO, and the relatively strong (0001) peak demonstrates the preferred orientation of the as-grown NWs.

In order to characterize the electrical performance of the P-doped ZnO NWs, ZnO NW field effect transistors (ZnO NWFET) were fabricated using a focused ion beam. P-doped ZnO NWs were spread on a p+ silicon wafer with a 100 nm thick silicon oxide on the top; the p+ Si substrate served as the back-gate electrode. The platinum (Pt) electrodes were

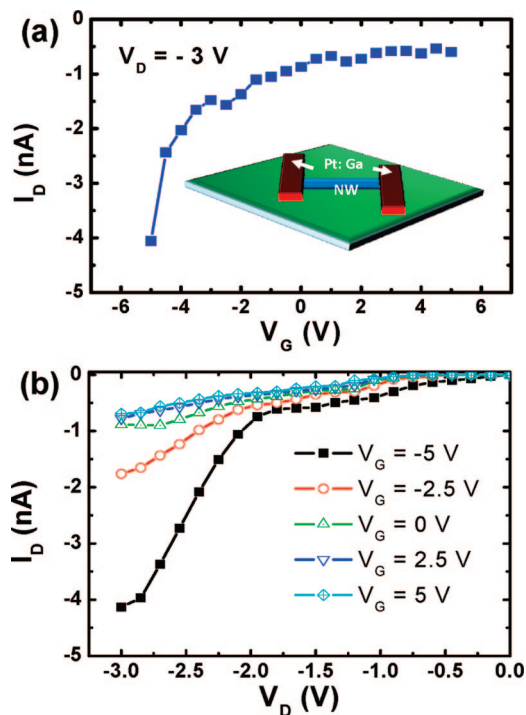


Figure 2. Electrical characteristics of P-doped ZnO NWFET. (a) The I_D – V_G curve of a P-doped NWFET at $V_D = -3$ V. The schematic diagram of the NWFET is shown in the inset. The electrodes at both ends of a single NW were deposited by FIB. (b) The I_D – V_D curves of P-doped NWFET with gate voltage (V_G) at -5 , -2.5 , 0 , 2.5 , and 5 V.

connected at each end of the single NW. In this experiment, the connecting electrodes of ZnO devices were deposited with a careful control to reduce the bombardment damage and contamination by Ga ions at ZnO NW. Importantly, ZnO NWs were stored in the ambient environment for about 1 month before fabricating to ZnO FETs. All electrical characteristics in this study were measured at room temperature under ambient conditions. The source and drain electrodes were connected to ground (V_S) and negative voltage (V_D), respectively. The gate voltage (V_G) was applied to the back-gate electrode to control the carrier density in ZnO NW. The gate-sweeping I – V characteristic of NWFET at a constant drain voltage ($V_D = -3$ V) is given in Figure 2a. Clearly, the absolute value of drain current is increasing with decreasing gate voltage from positive regime to negative regime. The result indicates that the ZnO NW is p-type. The hole density (p) per unit length in NW can be estimated by using the capacitive equation as

$$p = C_{\text{eff}} V_{\text{gt}} / q \quad (1)$$

where C_{eff} is the effective capacitance per unit length of the NWFET and V_{gt} is the threshold voltage of the ZnO NWFET.¹² The effective capacitance per unit length of NW can be written as $C_{\text{eff}} \sim 2\pi\epsilon\epsilon_0/\ln(4h/d)$, where d , h , and ϵ are the NW diameter, the thickness of dielectric layer, and the effective dielectric constant, respectively. From eq 1, the hole density can be calculated as $\sim(1-2.3) \times 10^7 \text{ cm}^{-1}$ ($\sim(0.3-0.9) \times 10^{17} \text{ cm}^{-3}$). The mobility can be calculated by using $\mu = g_m L / C_{\text{eff}} V_D$, where L is channel length, g_m is transconductance, and μ is mobility. The mobility is extracted in the range of $0.2-0.5 \text{ cm}^2/(\text{V s})$ from our experimental

result. According to the previous study, it is suggested that the formation of $[P_{zn}-2V_{zn}]$ complex in P-doped NWs is more favorable than P_o , in the oxygen-rich growth condition using Zn_3P_2 as dopant source. The $[P_{zn}-2V_{zn}]$ complex will play a role of dominant acceptor in ZnO NWs, which consists of a P dopant at Zn antisite and two Zn vacancies.¹¹ Consequently, it will have a lower mobility caused by more defects and scattering centers in P-doped ZnO NW.^{12,13} The mobility in this work is comparable to the report of phosphorus-doped ZnO NW.¹² Figure 2b shows the typical electrical characteristic of a p-type ZnO NWFET at different gate voltages. It demonstrates that the transport current in a NW can be modulated by gate voltage as a field effect transistor.

The piezoelectric response of the p-type NWs was measured using an atomic force microscope (AFM) (Molecular Force Probe MFP-3D from Asylum Research) with a Pt-coated Si tip.¹ In the AFM contact mode, a constant normal force of 5 nN was kept between the tip and sample surface. The output voltage across an outside load of resistance $R_L = 500\text{ M}\Omega$ was continuously monitored as the tip scanned across the NW array, with the bottom conductive film on the substrate being grounded. No external voltage was applied in any stage of the experiment. The spring constant of the cantilever was calibrated to be 2.02 N/m. The rectangular cantilever used for the measurements had a tetrahedral shape with an apex angle of 70° . Both the topography (feedback signal from the scanner) and the corresponding output voltage (V_L) images across the load were recorded simultaneously when the AFM tip was scanned over the aligned NW arrays. In contact mode, as the tip scanned over the vertically aligned NWs, the NWs were bent consecutively. In the output voltage image, many sharp output voltage peaks were observed, which resulted from the piezoelectric potential driven transient flow of electrons across the load as the tip consecutively scanned across the NW array.

Figure 3a is a 3D electrical image after scanning an area of $20\ \mu\text{m} \times 20\ \mu\text{m}$ over the p-type ZnO NW array. Figure 3b is a comparison of line scan topography image (dark curve) and the corresponding output voltage profile (blue curve) when the AFM tip scanned over p-type ZnO NWs. The electric output of the p-type NWs has two important characteristics. Almost all of the electrical pulses are positive with an average magnitude around 10–15 mV, and some peaks are as high as 50–90 mV. As for a single NW, an electrical pulse is generated when the p-type ZnO NW is bent without crossing the top of the NW, which is indicated by the relative position of the voltage peak in reference to the profile of the topological image.

To understand the piezoelectric characteristic of a p-type NW, we have calculated the piezoelectric potential in a bent p-type NW taking a finite carrier density into consideration. For a laterally bent ZnO NW without any doping, the stretched side exhibiting positive piezoelectric potential and the compressed side negative piezoelectric potential.^{3,14} With a finite p-type doping, the holes tend to accumulate at the negative piezoelectric potential side. The negative side is thus partially screened by holes while the positive side of the

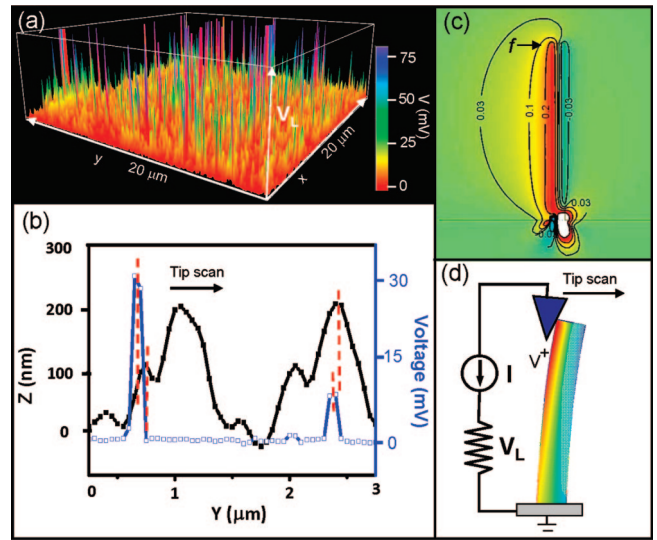


Figure 3. Piezoelectric power generation using the p-type ZnO NW arrays. (a) Three-dimensional plot of the output voltage at an external load records when the AFM tip scanned across the NW arrays. (b) A typical line scan profile from the AFM topography (black) and the corresponding output voltage (blue) images presented in (a). (c) Calculated piezoelectric potential distribution for the p-type NW with a doping concentration of $1 \times 10^{17}\text{ cm}^{-3}$. Details about the calculation are given in Supporting Information. For easy presentation, the bending shape of the nanowire is not presented. Besides the color plot, equipotential contours for $\varphi = -0.03, 0.03, 0.1, \text{ and } 0.2\text{ V}$ are also superimposed. The dimension of the nanowire is radius $a = 25\text{ nm}$ and $l = 600\text{ nm}$ and the external force is $f = 80\text{ nN}$. (d) Schematic for understanding the electricity output characteristics of the p-type ZnO NW.

piezoelectric potential preserves.¹⁵ Using the Poisson equation and the statistical Fermi–Dirac distribution of charge carriers (see Supporting Information and ref 15), for a typical ZnO NW with diameter 50 nm, length 600 nm, acceptor concentration $N_A = 1 \times 10^{17}\text{ cm}^{-3}$ under a bending force of 80 nN, the piezoelectric potential in the negative side is $> -0.05\text{ V}$ and is $\sim 0.3\text{ V}$ at the positive side (Figure 3c).

The mechanism for the piezoelectric voltage output of a p-type NW is illustrated in Figure 3d. When AFM tip scans and bends the NW, the deformation along the stretched side is slightly positive in reference to the ground root of the NW. As the NW is further bent and before the AFM tip runs across the top of the NW, as soon as the positive potential along the stretched side of the NW is strong enough to overcome a threshold, the positive piezopotential will drive the flow of the charge carriers through the external circuit, resulting in a positive output voltage peak since the transient current flows from the load to the grounded side.

The model shown in Figure 3d works if the negative potential at the compressed side is almost completely screened by the charge carriers, which is possible if the doping level is reasonably high. In a case where the piezoelectric charges are partially screened by free carriers that have a relatively low doping level, a presence of a Schottky barrier between the tip and NW is required to rectify the flow of charge carriers. As a result, the current can only flow in the direction along which the Schottky barrier is at forward bias. For a metal–p-type semiconductor contact, the

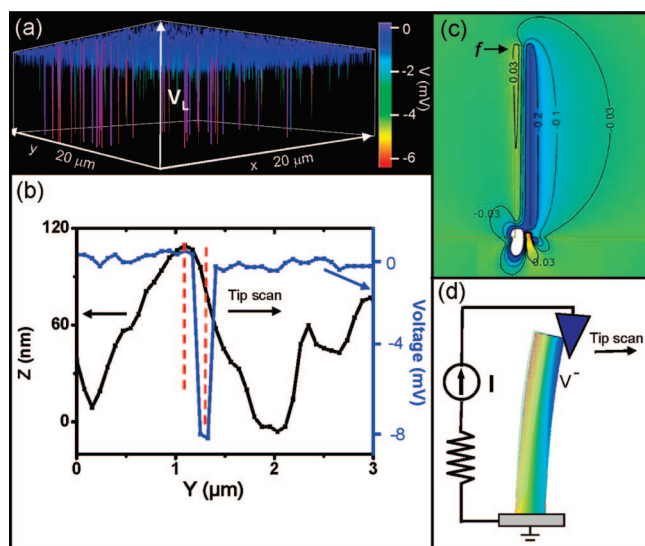


Figure 4. Piezoelectric power generation using the n-type ZnO NW arrays. (a) Three dimensional plot of the output voltage at an external load records when the AFM tip scanned across the NW arrays. (b) A typical line scan from the AFM topography (black) and the corresponding output voltage (blue) images presented in (a). (c) Calculated piezoelectric potential distribution for the n-type NW with a doping concentration of $1 \times 10^{17} \text{ cm}^{-3}$. Details about the calculation are given in ref 15. For easy presentation, the bending shape of the nanowire is not presented. Besides the color plot, equipotential contours for $\varphi = 0.03, -0.03, -0.1, \text{ and } -0.2 \text{ V}$ are also superimposed. The dimension of the nanowire is radius $a = 25 \text{ nm}$, $l = 600 \text{ nm}$, and the external force is $f = 80 \text{ nN}$. (d) Schematic for understanding the electricity output characteristics of the n-type ZnO NW.

Schottky barrier at the interface is at forward bias if the semiconductor has a higher potential, otherwise it is reversely biased. Transport measurement of the AFM Si/Pt tip–p-type NW showed a Schottky behavior (Figure S2 in Supporting Information). If we have millions of NWs that generate electricity simultaneously, the Schottky barrier makes all of the generated currents add up constructively and flow in the same direction.⁵

To confirm the signal observed for p-type ZnO NWs, we have carried out the experiments using the same AFM tip, the same equipment, under same conditions, and at almost the same time, but replacing the p-type ZnO NWs with n-type ZnO NWs. Figure 4a is a 3D output voltage profile generated by scanning the n-type ZnO NW arrays sample. Most of the potential pulses are around -5 to -10 mV . The output signal exhibits two distinct characteristics in comparison to that for the p-type NWs. The piezoelectric output pulses generated by the n-type ZnO NWs are always negative. More importantly, the position of the output voltage peak (blue curve) exhibits a delay in comparison to the topography profile (dark curve) (Figure 4b), indicating that the output voltage is generated when the tip touches the compressed side of the NW.

To explain the observed voltage output characteristics of the n-type NWs, we have investigated the behavior of free charge carriers in a bent piezoelectric semiconductive NW under thermodynamic equilibrium condition (Figure 4c).¹⁵ For a laterally bent n-type ZnO NW, with the stretched side

exhibiting positive piezoelectric potential and the compressed side negative piezoelectric potential, the conduction band electrons tend to accumulate at the positive side. The positive side is thus partially screened by free charge carriers while the negative side of the piezoelectric potential preserves as long as the donor concentration is not too high. For a typical ZnO NW with diameter 50 nm , length 600 nm , donor concentration $N_D = 1 \times 10^{17} \text{ cm}^{-3}$ under a bending force of 80 nN , the potential in the positive side is $<0.05 \text{ V}$ and is $\sim -0.3 \text{ V}$ at the negative side.

The mechanism of the electrical pulse generation by n-type ZnO NWs is illustrated in Figure 4d. When the n-type ZnO NW is bent by the AFM tip, positive potential and negative potential are created along stretched side and compressed side of the NW, respectively. If a small positive piezoelectric potential remains due to the incomplete screening of the piezoelectric charges by the free electrons, the presence of a reversely biased Schottky barrier (with the metal side has a lower potential than the semiconductor) prevents the flow of electrons across the interface. When the tip scans the top of the NW and touches the compressed side of the NW, the negative piezoelectric potential sets the Schottky barrier to forward bias, thus the free electrons can flow across the interface, resulting in a transient current in the external load. This is possible only when the tip touches the compressed side of the NW, in agreement to the experimental result shown in Figure 4b. The presence of the Schottky barrier forces the current to flow in the direction along which the Schottky barrier is at forward bias. If we have millions of NWs that generate electricity simultaneously, the Schottky barrier makes all of the generated currents add up constructively and flow in the same direction.⁵

In order to investigate the power generating details of p-type ZnO NWs, experiments have been carried out by changing scanning parameters of the AFM but using the same piece of sample. By scanning a fixed area of $20 \mu\text{m} \times 20 \mu\text{m}$ and counting the number of output voltage peaks and the average magnitude of the voltage peaks, we can understand some of the details about the energy generation. At a fixed contact force, with the increase of the scanning frequency, e.g., the increase in scanning speed, both the number of output voltage peaks and their average magnitude increase almost linearly (Figure 5a). This is possibly due to a fast straining of the NW results in a fast charging flow rate.¹⁶ A fast scan may also increase the frequency of reaching the NWs of slightly different heights by the AFM tip.

At a fixed scanning rate, an increase of normal contact force makes it possible to bend the NWs that have smaller lengths, resulting in an increase in the number of output voltage peaks (Figure 5b). But the dependence of the average magnitude of the output electrical pulses on the applied normal force is a bit complex. As the normal forces increased from 90 to 120 nN , the average magnitude of the output electrical pulses decreased. As the normal force increased from 170 to 230 nN , the average magnitude of the output electrical pulses increased from 6.4 to 9 mV . Although the degree of bending of a NW should increase theoretically with the increase in the applied force, but an increased contact

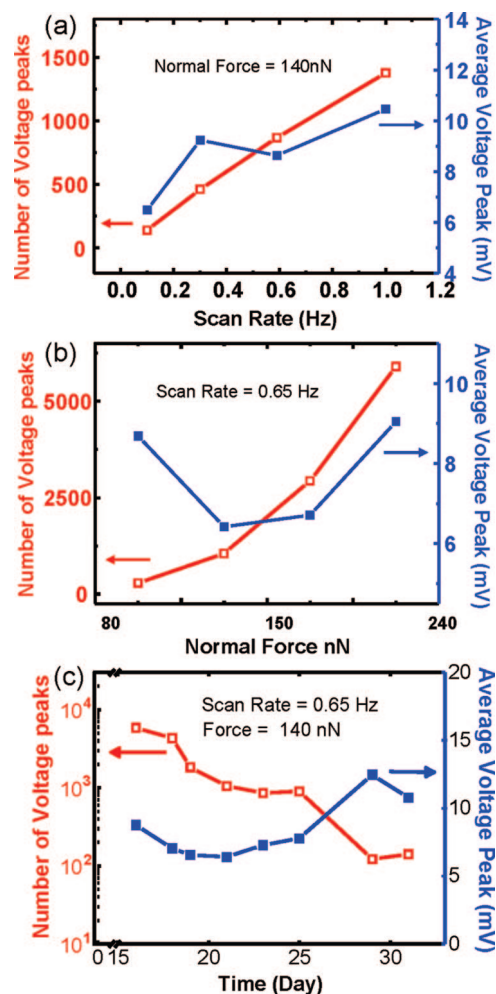


Figure 5. Statistics of piezoelectric output of the p-type NW arrays under different AFM scanning parameters. (a) The average number of voltage peaks (left axis, red square) and average magnitude of output voltage (right axis, blue solid square) under different AFM line scan rate. (b) The average number of voltage peaks (left axis, red square) and average magnitude of output voltage (right axis, blue solid square) under different normal contact forces. (c) The average number of voltage peaks (left axis, red square) and average magnitude of output voltage (right axis, blue solid square) as a function of time in days for testing the stability of the p-type NWs. Using the maximum number of peaks presented by the data here, it can be estimated that about 60% of the NWs produced output voltage.

force could force the NW to slide around the tip during experiment, possibly resulting in a decrease in magnitude of the measured output voltage peak.

We have examined the stability of the p-type NWs by measuring the piezoelectric output voltage as a function of time. The first measurement was done 16 days after the sample was synthesized (Figure 5c). (The samples were synthesized in Taiwan and the measurement was done in Georgia Tech.) After measuring the same sample for multiple of times until 32 days since its synthesis, the average magnitude of the output voltage peaks did not drop dramatically, but the number of the output voltage peaks dropped for close to 2 orders of magnitude. This drastic drop in the effectiveness of the NWs for generating electricity may be related to the instability of the p-type doping.

In summary, this paper presents the synthesis of phosphorus-doped ZnO nanowire arrays, which grew vertically on (001) silicon substrates. The orientation relationship and the structure of the NWs have been characterized using high-resolution TEM: $\text{Si}(001) \parallel \text{ZnO}(0001)$, $\text{Si}[1\bar{1}2] \parallel \text{ZnO}[01\bar{1}0]$, $\text{Si}[110] \parallel \text{ZnO}[2\bar{1}10]$. Transport measurement of the field effect transistor fabricated using the P:ZnO NWs showed that the NWs are p-type with a hole density of unit length $\sim(1-2.3) \times 10^7 \text{cm}^{-1}$, and mobility $0.2-0.5 \text{cm}^2/(\text{V s})$. With a conductive AFM in contact mode, energy conversion using the p-type ZnO NWs has been demonstrated for the first time. The p-type ZnO NWs produce positive piezoelectric output voltage as high as up to 50–90 mV once it is bent by an AFM tip, and the voltage pulse is generated when the tip contacts the stretched side (positive potential side) of the NW. In comparison, the n-type ZnO NW produces negative piezoelectric output voltage in the range of -5 to -10 mV when subject to AFM deformation, and the voltage pulse is generated when the tip contacts the compressed side (negative potential side) of the NW. These experimental observed phenomena have been fully explained based on the mechanism proposed for nanogenerator.^{4,8}

Acknowledgment. Research supported by DARPA (Army/AMCOM/REDSTONE AR, W31P4Q-08-1-0009), Air Force Office (FA9550-08-1-0446), KAUST Global Research Partnership, and National Science Council (NSC 97-2120-M-007-003). Thanks to Chen Xu and Chun-Chi Chen for technical assistance.

Supporting Information Available: Figures showing a TEM image of the interface between the p-type NWs and the Si(001) substrate and transport measurement between the AFM tip Si/Pt and the p-type NWs and description of calculation of the piezoelectric potential distribution in a p-type nanowire with finite doping. This material is available free of charge via the Internet at <http://pubs.acs.org>.

References

- (1) Tian, B.; Zheng, X.; Kempa, T. J.; Fang, Y.; Yu, N.; Yu, G.; Huang, J.; Lieber, C. M. *Nature* **2007**, *449*, 885.
- (2) Tian, B.; Kempa, T. J.; Lieber, C. M. *Chem. Soc. Rev.* **2009**, *38*, 16.
- (3) Kempa, T. J.; Tian, B.; Kim, D. R.; Hu, J.; Zheng, X.; Lieber, C. M. *Nano Lett.* **2008**, *8*, 3456.
- (4) Wang, Z. L.; Song, J. H. *Science* **2006**, *312*, 242.
- (5) Wang, X. D.; Song, J. H.; Liu, J.; Wang, Z. L. *Science* **2007**, *316*, 102.
- (6) Qin, Y.; Wang, X. D.; Wang, Z. L. *Nature* **2008**, *451*, 809.
- (7) Xu, S.; Wei, Y.; Liu, J.; Yang, R.; Wang, Z. L. *Nano Lett.* **2008**, *8*, 4027.
- (8) Wang, Z. L. *Adv. Func. Mater.* **2008**, *18*, 1.
- (9) Wang, Z. L. *Sci. Am.* **2008**, *298*, 82.
- (10) Park, C. H.; Zhang, S. B.; Wei, S. H. *Phys. Rev. B* **2002**, *66*, 073202.
- (11) Lee, W. J.; Kang, J.; Chang, K. J. *Phys. Rev. B* **2006**, *73*, 024117.
- (12) Xiang, B.; Wang, P.; Zhang, X.; Dayeh, S. A.; Aplin, D. P. R.; Soci, C.; Yu, D.; Wang, D. *Nano Lett.* **2007**, *7*, 323.
- (13) Yuan, G. D.; Zhang, W. J.; Jie, J. S.; Fan, X.; Zapfen, J. A.; Leung, Y. H.; Luo, L. B.; Wang, P. F.; Lee, C. S.; Lee, S. T. *Nano Lett.* **2008**, *8*, 2591.
- (14) Gao, Y. F.; Wang, Z. L. *Nano Lett.* **2007**, *7*, 2499.
- (15) Gao, Y. F.; Wang, Z. L. *Nano Lett.* **2009**, published online, DOI: 10.1021/nl803547f.
- (16) Yang, R. S.; Qin, Y.; Dai, L. M.; Wang, Z. L. *Nat. Nanotechnol.* **2008**, *4*, 34.

NL900115Y